$EuAg_xAl_{11-x}$ with the $BaCd_{11}$-Type Structure: Phase Width, Coloring, and Electronic Structure

Fei Wang,[†] Karen Nordell Pearson,[‡] and Gordon J. Miller*,[†]

Department of Chemistry, Iowa State University, Ames, Iowa 50011, and Department of Chemistry, Lawrence University, Appleton, Wisconsin 54912

Received November 6, 2008. Revised Manuscript Received December 3, 2008

The $EuAg_xAl_{11-x}$ (loading composition, $x \approx 3-8$) ternary system was experimentally and theoretically investigated. According to powder X-ray diffraction, phases adopting the $BaCd_{11}$-type structure (space group $I4_1/amd$, $Z = 4$) were obtained for a narrow composition range, i.e., $x \approx 5-6$. Single-crystal X-ray crystallography showed that Ag and Al atoms share 4b, 8d, and 32i sites and that 4b site distinctly prefers Ag to Al. Eu is divalent in these phases, which was supported by both magnetometry and unit-cell dimensional analysis. Comparison with other isostructural RE (rare earth)−Ag−Al compounds showed that the $BaCd_{11}$-type structure is stable specifically at the valence electron concentrations (vec) of 2.1−2.3 e^- per atom. A Mulliken population analysis was performed with Extended Hückel calculations, the result of which explained the observed site preferences of the Ag and Al atoms. TB-LMTO-ASA calculations were used to study the relative energies of various models established according to crystallography and the coloring problem was included by maximizing the number of Ag−Al contacts. The calculated density of states (DOS) and crystal orbital Hamiltonian population (COHP) curves explain the stability of the $BaCd_{11}$-type structure at specifically vec $\approx$ 2.1−2.3 e^- per atom in RE−Ag−Al ternary compounds.

Introduction

Polar intermetallic compounds are an emerging group of inorganic solids attracting attention for their chemical and physical characteristics. They are composed of electropositive metals (e.g., alkali metals, alkaline earth metals, and rare earth metals) and electronegative metals (i.e., metals around the Zintl border),[1−3] representing an intermediate compound class between classical intermetallic phases, such as Hume−Rothery and Laves phases on the one hand,[4] and valence compounds, e.g., Zintl phases,[5] on the other. Polar intermetallics often form complex structures, such as $NaZn_{13}$-, $BaCd_{11}$-, or $BaHg_{11}$-types, which can be significantly different from those of the component metals. Their chemical bonding characteristics also represent a complex interplay among metallic, covalent, and ionic bonding. Such features of polar intermetallics lead to many extraordinary properties, such as enhanced magnetocaloric effects[6] and superconductivity.[7] From the chemical perspective, polar intermetallics provide a structural and electronic framework for two electronegative elements, which by themselves show no binary phases in their equilibrium phase diagrams, to combine, as for example, Sn and Ge or In and Ge.[8,9] To exploit these properties and design new polar intermetallic materials, it is essential to understand the composition−structure−property relationship in these compounds. The valence electron counting rules, such as those adopted for Hume−Rothery phases[4] and the octet rule for Zintl phases,[5] are insufficiently effective for these intermediate cases. Therefore, new rules need to be established through further systematic investigations into polar intermetallics.

The RE (rare earth)−Ag−Al systems have been extensively investigated in part because of their structural richness.[10] Among these kaleidoscopic complex structures obtained at various compositions, site sharing between Ag and Al atoms and specific site preferences are commonly observed. Therefore, a thorough investigation into RE−Ag−Al ternary systems will largely enrich our understanding of the

* Corresponding author. E-mail: gmiller@iastate.edu.
[†] Iowa State University.
[‡] Lawrence University.

(1) Schäfer, H. *Annu. Rev. Mater. Sci.* **1985**, *5*, 1.
(2) Häussermann, U.; Amerioun, S.; Eriksson, L.; Lee, C.-S.; Miller, G. J. *J. Am. Chem. Soc.* **2002**, *124*, 4371.
(3) You, T. S.; Grin, Y.; Miller, G. J. *Inorg. Chem.* **2007**, *46*, 8801.
(4) Hume-Rothery, W.; Raynor, G. V. *The Structure of Metals and Alloys*, 1st ed; The Institute of Metals: London, 1936.
(5) Schäfer, H.; Eisenmann, B.; Müller, W. *Angew. Chem., Int. Ed.* **1973**, *12* (9), 694.
(6) Gschneidner Jr, K. A.; Pecharsky, V. K.; Tsokol, A. O. *Rep. Prog. Phys.* **2005**, *68*, 1479.
(7) Curro, N. J.; Caldwell, T.; Bauer, E. D.; Morales, L. A.; Graf, M. J.; Bang, Y.; Balatsky, A. V.; Thompson, J. D.; Sarrao, J. L. *Nature* **2005**, *434*, 622.
(8) Zürcher, F.; Nesper, R.; Hoffmann, S.; Fässler, T. F. *Z. Anorg. Allg. Chem.* **2001**, *627* (9), 2211.
(9) Tobash, P. H.; Lins, D.; Bobev, S. *Chem. Mater.* **2005**, *17* (22), 5567.
(10) (a) Denysyuk, O. V.; Stel'makhovych, B. M.; Kuz'ma, Yu. B. *J. Solid State Chem.* **1994**, *109*, 172. (b) Stel'makhovych, B. M.; Kuz'ma, Yu. B. *Dopov. Akad. Nauk Ukr.* **1994**, *3*, 86. (c) Zhak, O. V.; Stel'makhovych, B. M.; Kuz'ma, Yu. B. *Russ. Metall.* **1995**, *6*, 158. (d) Kuz'ma, Yu. B.; Zhak, O. V.; Shkolyk, S. Yu. *Dopov. Akad. Nauk Ukr.* **1995**, *3*, 101. (e) Zhak, O. V.; Stel'makhovych, B. M.; Kuz'ma Yu, B *J. Alloys Compd.* **1996**, *237*, 144. (f) Kuz'ma Yu, B.; Zhak, O. V.; Sarapina, O. S. *Russ. Metall.* **1997**, *2*, 166. (g) Zhak, O. V.; Kuz'ma, Yu. B. *J. Alloys Compd.* **1999**, *291*, 175. (h) Stel'makhovych, B. M.; Gumenyuk, T. M.; Kuz'ma, Yu. B. *J. Alloys Compd.* **2000**, *298*, 164. (i) Gumeniuk, R. V.; Stel'makhovych, B. M.; Kuz'ma, Yu. B. *J. Alloys Compd.* **2001**, *321*, 132. (j) Stel'makhovych, B. M.; Zhak, O. V.; Bilas, N. R.; Kuz'ma, Yu. B. *J. Alloys Compd.* **2004**, *363*, 243. (k) Cordier, G.; Dörsam, G.; Kniep, R. *J. Magn. Magn. Mater.* **1988**, *76 & 77*, 653.

10.1021/cm803021u CCC: $40.75
Published on Web 01/05/2009

Table 1. Phases Formed in the Arc Melted Samples

loading composition	$Eu(Ag,Al)_{11}$ ($BaCd_{11}$)	$Eu(Ag,Al)_{11}$ ($BaHg_{11}$)	$Eu_2(Ag,Al)_{17}$ (Th_2Ni_{17})	$Eu_2(Ag,Al)_{17}$ (Th_2Zn_{17})	$Eu(Ag,Al)_4$ ($BaAl_4$)	$(Ag,Al)_1$ (fcc)
$EuAg_3Al_8$	+	+	+		+	+
$EuAg_4Al_7$	+	+			+	+
$EuAg_5Al_6$	+					
$EuAg_6Al_5$	+					
$EuAg_7Al_4$	+			+		+
$EuAg_8Al_3$	+			+		+

composition−structure−property relationship in polar intermetallics. However, although synthetic and crystallographic studies have been the major focus thus far for these systems, theoretical investigations have rarely been done. Many questions remain, for example, on the factors influencing the arrangements and distributions of Ag and Al atoms in these intermetallics. Furthermore, we believe that a synergistic effort between experiment and theory will be critical to elucidate the broader relationships needed to successfully target and obtain desired intermetallic systems.

This work involves a part of our efforts devoted to the $EuAg_xAl_{11-x}$ ternary system. Specifically, we will focus on phases adopting the $BaCd_{11}$-type structure. This structure has been reported for many binary phases, such as $SrCd_{11}$, $CeZn_{11}$,[11] and $SrZn_{11}$,[12] showing valence electron concentration (vec) slightly greater than 2.00 e^- per atom. The stability of this structure for specific pairs of elements relies significantly on atomic size. Iandelli and Palenzona showed that, for RE−Zn binary systems, the $BaCd_{11}$-type structure occurs when RE = La, Ce, Pr, Nd, Eu, and Yb, but cannot be obtained with smaller (late) RE atoms.[13] Eu and Yb are exceptions because they are divalent and their sizes are comparable with the early trivalent RE atoms. Meanwhile, the number of valence electrons also plays an important role. Hückel-type calculations revealed that the $BaCd_{11}$-type structure is the most stabilized at the vec value of 2.1 e^- per atom.[14] In $EuAg_xAl_{11-x}$, by varying the composition, we can tune the number of valence electrons. So the theoretical conclusion can be experimentally tested here.

In this work, both experimental and theoretical investigations were carried out for the $BaCd_{11}$-type $EuAg_xAl_{11-x}$ ternary phases to answer the following questions: (i) at what compositions (and valence electron concentrations) can this phase be obtained; (ii) how are Ag and Al atoms distributed among the various sites in the crystal structure; and (iii) what are the electronic structures and bonding characteristics in these phases and what can be rationalized from them.

Experimental Section

Syntheses. $EuAg_xAl_{11-x}$ specimens were synthesized from the pure metals: Eu (rods, Ames Laboratory, 99.99%), Ag (slugs, Alfa Aesar, 99.99%), and Al (foil, Tenneco). Both our previous study[15] and Denysyuk's report[10a] showed that a single phase with the $BaCd_{11}$-type structure can be obtained at the composition around $EuAg_5Al_6$. To investigate the homogeneity width for these $BaCd_{11}$-type phases, we mixed the metals with a series of Eu:Ag:Al molar ratios varying from 1:3:8 to 1:8:3. This composition range, shown later by crystallographic results, is sufficiently large to cover the homogeneity width. Approximately 0.5 g of each mixture was arc-melted under a high purity argon atmosphere. To ensure thorough reaction, we turned over every sample and remelted it five times. The weight loss during melting is between ca. 0.3 and 1.0 wt %. The products are all stable toward rapid decomposition in air and water, but react with 40 wt % nitric acid. After reaction, every product was broken into halves: one-half was submitted directly to characterization; the other half was sealed under argon in a tantalum tube, which was then sealed in a silica jacket under a vacuum and annealed at 500 °C for 40 days in a tube furnace before subsequent characterization.

X-Ray Crystallography. Powder X-ray diffraction (XRD) was used to identify the phases in each sample. It was carried out on a Huber Imaging Plate Guinier Camera G670 using monochromatized Cu $K\alpha_1$ radiation (λ = 1.54059 Å). The exposure time was 1 h and the step size was 0.005°. Full pattern decomposition was performed with the Le Bail technique[16] using the software LHPM-Rietica.[17]

For single-crystal XRD, small crystals were selected from crushed samples and glued on the tips of capillaries with epoxy. Diffraction was carried out at room temperature on a Bruker *SMART* Apex CCD diffractometer equipped with Mo $K\alpha$ radiation (λ = 0.71073 Å). The data collection was controlled with the *SMART* program.[18] Three sets of frames were collected at φ = 0, 120, and 240°. For every set, ω was scanned from 332.0 to 150.5° with the step size of 0.3°. The exposure time for every frame was 10 s. Data integrations, cell refinements, and absorption corrections were done with the SAINT+[19] and SADABS programs.[20] Using the SHELXTL package,[21] we then solved the crystal structures using direct methods and refined by full-matrix least-squares on F^2. More details about the refinement are listed in Table 2.

Magnetometry. A small piece (5.1 mg) was taken from the product with the loading composition $EuAg_5Al_6$, which is characterized as a $BaCd_{11}$-type "single phase" according to powder XRD. The temperature dependency of its magnetic susceptibility was measured on a Quantum Design MPMS XL superconducting quantum interference device (SQUID) magnetometer. The magnetic field was fixed at 1 kOe and the temperature was scanned from 5 to 300 K.

Electronic Structure Calculations. To rationalize site preferences for Ag and Al atoms, a Mulliken population analysis was

(11) Sanderson, M. J.; Baneziger, N. C. *Acta Crystallogr.* **1953**, *6*, 627.
(12) Kal, S.; Stoyanov, E.; Groy, T. L.; Häussermann, U. *Acta Crystallogr., Sect. C* **2007**, *63*, i96.
(13) Iandelli, A.; Palenzona, A. *J. Less-Common Met.* **1967**, *12*, 333.
(14) Häussermann, U.; Svensson, C.; Lidin, S. *J. Am. Chem. Soc.* **1998**, *120*, 3867.
(15) Nordell, K. J. Exploring Aluminum-Rich Intermetallics with Experiment and Theory. Ph.D. Thesis, Iowa State University, Ames, IA, 1997.
(16) Le Bail, A.; Duroy, H.; Fourquet, J. L. *Mater. Res. Bull.* **1988**, *23*, 447.
(17) Hunter, B. A.; Howard, C. J. *LHPM-Rietica*, version 1.71; Australian Nuclear Science and Technology Organization: Menai, Australia, 2000.
(18) *SMART*, version 5.625; Bruker AXS Inc.: Madison, WI, 2001.
(19) *SAINT+*, version 6.22; Bruker AXS Inc.: Madison, WI, 2001.
(20) *SADABS*, version 2.03; Bruker AXS Inc.: Madison, WI, 2001.
(21) *SHELXTL*, version 6.10; Bruker AXS Inc.: Madison, WI, 2000.

Table 2. Crystallographic Data and Selected Refinement Parameters of the Crystals Selected from $EuAg_5Al_6$ Samples (Both As-Cast and Annealed)

	as-cast	annealed
empirical formula	$EuAg_{5.07(4)}Al_{5.93(4)}$	$EuAg_{4.96(4)}Al_{6.04(4)}$
space group	$I4_1/amd$ (No. 141)	$I4_1/amd$ (No. 141)
a (Å)	11.0613(10)	11.0549(17)
c (Å)	7.1302(9)	7.1301(15)
V (Å^3)	872.40(16)	871.4(3)
Z	4	4
θ range (deg)	3.40−28.22	3.40−28.23
index ranges	$-14 \le h \le 14$ $-14 \le k \le 14$ $-9 \le l \le 9$	$-14 \le h \le 14$ $-11 \le k \le 14$ $-6 \le l \le 9$
no. of reflns collected	3504	2352
no. of independent reflns	297 (R_{int} = 0.0406)	298 (R_{int} = 0.0720)
GOF on F^2	1.140	1.020
final R indices ($I > 2\sigma(I)$)	R1 = 0.0173; wR2 = 0.0350	R1 = 0.0265; wR2 = 0.0427
R indices (all data)	R1 = 0.0206; wR2 = 0.0356	R1 = 0.0396; wR2 = 0.0468
largest diff. peak/hole	0.745/−0.918 e$^-$/Å^3	1.052/−1.099 e$^-$/Å^3

carried out using Extended Hückel calculations.[22] The basis set consisted of single-ζ Slater orbitals for Al 3s ($H_{3s-3s} = -11.84$ eV, $\zeta_{3s} = 1.51$) and 3p ($H_{3p-3p} = -5.99$ eV, $\zeta_{3p} = 1.17$), Ag 5s ($H_{5s-5s} = -7.58$ eV, $\zeta_{5s} = 1.82$) and 5p ($H_{5p-5p} = -3.97$ eV, $\zeta_{5p} = 1.27$), and Eu 6*s* ($H_{6s-6s} = -5.67$ eV, $\zeta_{6s} = 1.58$).[23] Integrated populations were obtained by using a special points set of 64 *k*-points in the irreducible wedge of the tetragonal Brillouin zone. Ag 4d and Eu 4f orbitals were treated as core orbitals and not included in the basis sets. These treatments were justified later by further experimental and theoretical investigations: (i) subsequent first principles, electronic structure calculations show that the Ag 4d bands are filled and located ca. 5 eV below the Fermi level; and (ii) both unit-cell dimensional analysis and magnetometry indicates that Eu behaves divalent with a half-filled, localized set of 4f orbitals. More details are given in the section on Mulliken Populations and Site Preferences.

First-principles electronic structure calculations were performed with the Stuttgart tight-binding, linear-muffin-tin Orbital program using the atomic sphere approximation (TB-LMTO-ASA).[24] The calculation models were established according to the single-crystal XRD results listed in Tables 2 and 3. Further details of the models are given in the section of Calculation Models and the Coloring Problem. The von Barth-Hedin local density approximation[25] was employed for the treatment of exchange and correlation energy. The basis set included the 6s, 6p (downfolded[26]), and 5d states of Eu; the 5s, 5p, and 4d states of Ag; and the 3s, 3p, and 3d (downfolded) states of Al. Again, the half-filled 4f states of Eu were treated as core states. The Wigner-Seitz radii of the atomic spheres were 2.32 Å for Eu and 1.53 Å for both Ag and Al, which filled the unit cell with a 7.76% overlap without introducing any empty spheres. 360 ($6 \times 6 \times 10$) *k*-points in the irreducible wedge of the tetragonal Brillouin zone were used for integration. The density of states (DOS) and various crystal orbital Hamiltonian populations (COHP)[27] were calculated and plotted.

Results and Discussions

X-ray Crystallography. By scanning the loaded composition in $EuAg_xAl_{11-x}$ from "$EuAg_3Al_8$" to "$EuAg_8Al_3$," we obtained seven phases, which are listed in Table 1. The powder XRD patterns of the as-cast and annealed samples for "$EuAg_5Al_6$" and "$EuAg_6Al_5$" are shown in Figure 1 (XRD patterns for samples having $x = 3$, 4, 7, and 8 are presented in the Supporting Information). This range in composition for $EuAg_xAl_{11-x}$ indicated competition between two different, iso-compositional structures, i.e., the $BaHg_{11}$- vs $BaCd_{11}$-types, and the Th_2Ni_{17}- vs Th_2Zn_{17}-types. These structure types occur frequently among the polar intermetallic compounds involving rare earth, late transition metals, and elements from group 13 or 14. Further investigations into these competitive structures will deepen our understanding into the composition−structure relationship of polar intermetallic compounds, which will be the topic of a subsequent paper.

Table 3. Atomic Coordinates and Isotropic Displacement Parameters of $EuAg_{5.07(4)}Al_{5.93(4)}$

atom	Wyck.	x	y	z	SOF	U_{iso} (Å^2)
Eu	4a	1/2	1/4	5/8	1	0.010(1)
Ag/Al1	4b	1/2	1/4	1/8	0.873/0.127(6)	0.015(1)
Ag/Al2	8d	1/2	1/2	0	0.458/0.542(4)	0.015(1)
Ag/Al3	32i	0.3802(1)	0.4558(1)	0.3260(1)	0.410/0.590(3)	0.014(1)

The $BaCd_{11}$-type phases occurred over the entire range of $x = 3-8$ in $EuAg_xAl_{11-x}$, but the "single phase" was only obtained with the arc-melted $EuAg_5Al_6$ and $EuAg_6Al_5$ specimens, in which no other phases were detected by powder XRD (Figure 1). These "single phases" remained stable during annealing: for $EuAg_5Al_6$, only one small additional peak (at $2\theta = 34.3°$, from a $BaHg_{11}$-type structure) appears after annealing (shown with the black arrow in Figure 1); and for $EuAg_6Al_5$, there is no perceptible change in the powder XRD pattern. This reveals that the phase width of the $BaCd_{11}$-type structure in $EuAg_xAl_{11-x}$ is very narrow, approximately $EuAg_5Al_6$−$EuAg_6Al_5$.

Crystals were selected from both as-cast and annealed portions of these two "single-phase" samples for single-crystal XRD. The results of refinement are included in both Table 2 (the $EuAg_5Al_6$ sample) and Table S1 (the $EuAg_6Al_5$ sample in the Supporting Information), from which we can see that the refined compositions are all close to the loading compositions. The atomic coordinates and isotropic thermal parameters of $EuAg_{5.07(4)}Al_{5.93(4)}$ are listed in Table 3. Selected interatomic distances are tabulated in Table 4. Just like in the Ag−Al binary phases and other RE(rare earth)−Ag−Al ternaries,[10] site sharing occurs between Ag and Al atoms, which may be attributed to the fact that Ag and Al have similar atomic sizes and electronegativities. Among the three shared sites in the asymmetric unit of $EuAg_{5.07(4)}Al_{5.93(4)}$, the occupancies of Ag and Al are close to each other on the 8d and 32i sites, but differ significantly on the 4b site, which evidently prefers Ag to Al. These various sites for Ag and Al atoms also show significant differences with respect to interatomic distances: Ag/Al−Ag/Al contacts involving the 4b sites are longer (ca. 2.90−3.00 Å), whereas those involving the 8d or 32i sites are significantly shorter (ranging from ca. 2.65−2.82 Å). These observed distances compare well with the shortest interatomic distances characterized in

(22) Hoffmann, R. *J. Chem. Phys.* **1963**, *39* (6), 1397.
(23) Herman, A. *Modelling Simul. Mater. Sci. Eng.* **2004**, *12*, 21.
(24) Jepsen, O.; Andersen O. K. *TB-LMTO*, version 47; Max-Planck-Institut für Festkörperforschung: Stuttgart, Germany, 2000.
(25) von Barth, U.; Hedin, L. *J. Phys. C: Solid State Phys.* **1972**, *5*, 1629.
(26) Lambrecht, W. R. L.; Andersen, O. K. *Phys. Rev. B* **1986**, *34*, 2439.
(27) Dronskowski, R.; Blöchl, P. *J. Phys. Chem.* **1993**, *97*, 8617.

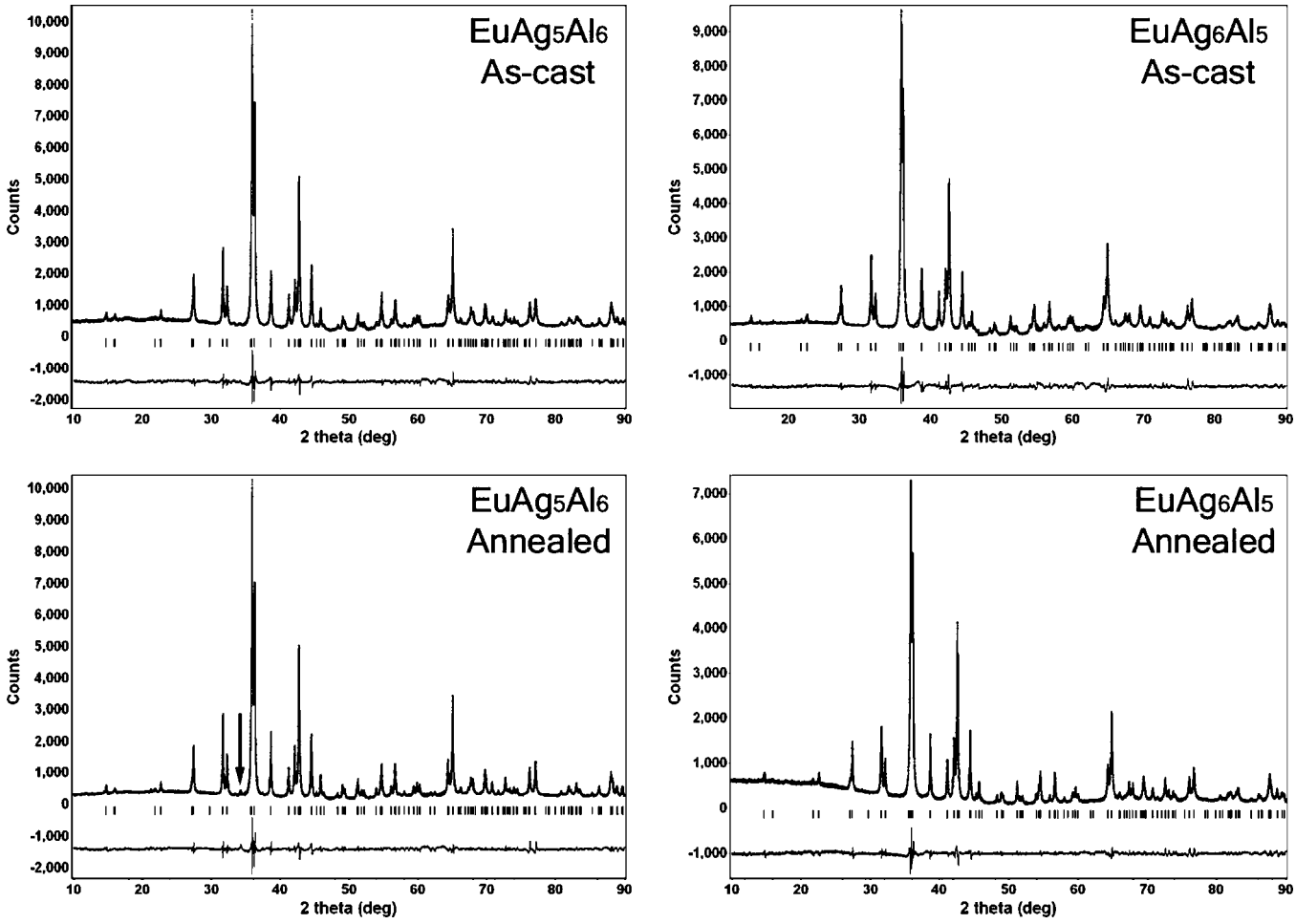

Figure 1. Powder patterns of the "single-phase" $BaCd_{11}$-type samples: $EuAg_5Al_6$ and $EuAg_6Al_5$. The small peak indicated with a black arrow in $EuAg_5Al_6$ (annealed) is from the $BaHg_{11}$-type structure.

Table 4. Selected Interatomic Distances of $EuAg_{5.07(4)}Al_{5.93(4)}$

atom pair		distances (Å)
Eu–	Ag/Al1 (× 2)	3.5651(5)
	Ag/Al2 (× 4)	3.8466(3)
	Ag/Al3 (× 8)	3.3886(6)
	(× 8)	3.5305(6)
Ag/Al1–	Ag/Al2 (× 4)	2.9054(2)
	Ag/Al3 (× 8)	2.9990(6)
Ag/Al2–	Ag/Al3 (× 4)	2.7199(6)
	(× 4)	2.7483(6)
Ag/Al3–	Ag/Al3 (× 1)	2.6495(11)
	(× 1)	2.6661(11)
	(× 2)	2.7938(6)
	(× 1)	2.8161(11)

the binary Ag−Al close-packed alloys by X-ray powder diffraction, distances which range from ca. 2.80−3.03 Å.[28]

The $BaCd_{11}$-type structure, which has been described by Häussermann et al.[14] and Pearson,[29] is shown in Figure 2. The Ag/Al2 (8d) and Ag/Al3 (32i) sites form strands of edge-sharing tetrahedron stars (Figure 2a), which are aligned along the crystallographic *c*-axis and interconnected with each other via the 8d sites. The channels confined by these strands are filled by Eu (4a) and Ag/Al1 (4b) sites (Figure 2b). The coordination environment of the Eu site, as shown in Figure 2c, consists of 22 Ag/Al atoms. Two Ag/Al1 atoms are located just above and below Eu along the *c*-axis. The

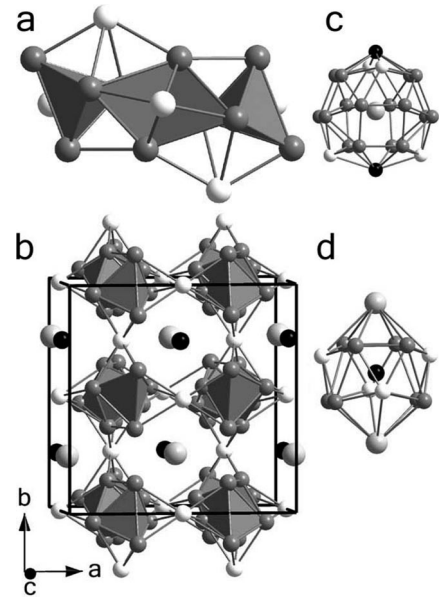

Figure 2. Crystal structure of $BaCd_{11}$-type $EuAg_xAl_{11-x}$. (a) Tetrahedron star strand; (b) unit cell projected along the *c*-axis; (c) coordination environment of Eu; (d) coordination environment of the Ag/Al1 site. Eu(4a), large gray; Ag/Al1(4b), small black; Ag/Al2(8d), small white; Ag/Al3(32i), small gray.

(28) (a) Neumann, J. P.; Chang, Y. A. *Trans. Metall. Soc. AIME* **1968**, *242*, 700. (b) Pradhan, S. K.; De, M. *J. Appl. Crystallogr.* **1986**, *19*, 484.

(29) Pearson, W. B. *Z. Kristallogr.* **1980**, *152*, 23.

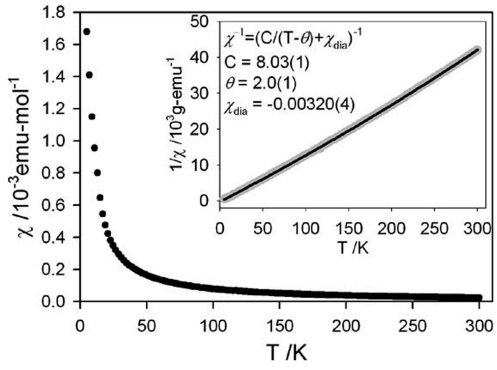

Figure 3. Temperature dependencies of the magnetic susceptibility and the reciprocal susceptibility of $BaCd_{11}$-type $EuAg_xAl_{11-x}$.

remaining 20 atoms form three rings: one in the middle is an 8-membered ring composed of Ag/Al3 atoms, which is "sandwiched" by two 6-membered rings, each composed of two Ag/Al2 atoms and four Ag/Al3 atoms. The coordination environment of the Ag/Al1 (*4b*) site is also shown in Figure 2d. Ag/Al1 lies between the two 6-membered rings mentioned above, which are capped by Eu atoms along the *c*-axis.

Magnetometry. The temperature dependencies of the magnetic susceptibility (χ) and the reciprocal susceptibility ($1/\chi$) of the $EuAg_5Al_6$ sample are plotted in Figure 3. It shows that this phase is paramagnetic from 5−300 K and follows a Curie−Weiss behavior. Fitting the $1/\chi$ vs T curve according to the Van Vleck equation gave the effective moment $\mu_{eff} = 8.01\ \mu_B$. This value is comparable with the effective moments reported for EuPtIn ($8.0\ \mu_B$)[30] and EuAgSn ($7.97\ \mu_B$).[31] It is close to the theoretical value of free Eu^{2+} ($7.94\ \mu_B$). So it can be concluded that Eu is divalent in these phases.

Comparison with Other $REAg_xAl_{11-x}$. Besides Eu, the $BaCd_{11}$-type structure was also reported for La, Ce, and Pr systems.[10] The compositions, lattice parameters, and unit cell volumes of these isostructural phases are compared in Table 5. The unit cell volume decreases as the RE atom varies from La to Ce to Pr, in accordance with the decreasing sizes of the RE atoms, but abruptly increases at Eu. This confirms that Eu is divalent in the $BaCd_{11}$-type phases and the other RE atoms are trivalent.

A comparison of their compositions shows that the Eu phases have higher Al contents than the trivalent La, Ce, and Pr counterparts. This compositional discrepancy, however, leads to a consistency in the valence electron concentration (vec), which is calculated with the total valence electron count divided by the number of electronegative metal atoms, e.g. for $EuAg_6Al_5$, vec $= 23/11 \approx 2.09\ e^-$ per atom (Ag 4d electrons are considered as core electrons, and ignored for electron counting purposes).

The calculated vec values for the observed phases are also listed in Table 5, all of which fall between 2.1 and 2.3 e^- per atom, which is in agreement with the previously reported 2.1 electrons per atom from Hückel calculation,[14] and yet confirms that this narrow vec range specifically stabilizes the $BaCd_{11}$-type structure for the RE−Ag-Al system. Similar to RE−Zn systems,[13] for RE−Ag-Al, the atomic sizes of the RE atoms significantly affect the stability of the $BaCd_{11}$-structure, as it cannot be obtained with smaller and later RE atoms except for Yb (again, due to its divalency).[10]

Mulliken Population and Site Preferences. Site preferences for different elements in a chemical structure can be rationalized through a Mulliken population analysis upon uniform reference frames.[32,33] Two uniform reference frames, i.e., $EuAg_{11}$ and $EuAl_{11}$, were established according to the crystallographic results. All Ag/Al mixed sites were assigned to Ag atoms in $EuAg_{11}$ and to Al in $EuAl_{11}$. Mulliken populations were calculated at 24 valence electrons per formula unit (vec $= 24/11 \approx 2.2\ e^-$ per atom) and tabulated in Table 6. These results show that among the 4b, 8d, and 32i sites in the $BaCd_{11}$-type structure, the 4b site has the lowest Mulliken population in both uniform reference frames. Therefore, it is energetically favorable to put the atom with higher-energy valence orbitals on this 4b site, which can explain why the 4b site prefers Ag atoms to Al atoms.

Computational Models and the Coloring Problem. To build the computational models with compositions close to $EuAg_5Al_6$ and $EuAg_6Al_5$ and to include the site sharing by Ag and Al atoms among the crystallographic sites as obtained from the refinements of single crystal XRD experiments, symmetry reduction is required. For example, to build a model with the composition $EuAg_6Al_5$, we can reduce the tetragonal symmetry to triclinic (space group $P1$) so that the 4b, 8d, and 32i sites can be broken into 44 independent 1a sites, 24 of which can be assigned to Ag and the other 20 to Al. The remaining challenge here is the "coloring problem",[33] i.e., there are multiple ways to assign the mixed sites to Ag and Al atoms. Four randomly chosen coloring schemes, numbered as models **1**−**4** and differentiated by their coordination environments at Eu, are illustrated in Figure 4a−d, all of which give the same composition, $EuAg_6Al_5$. To build computational models for chemical bonding analysis via DOS and COHP curves, we must first determine the appropriate coloring schemes.

The coloring schemes that give the lowest theoretically determined total energies are the most desirable models to compare against experimental results. To locate such coloring schemes, first-principles calculations were performed at first upon models **1**−**4** using TB-LMTO-ASA. These results are sorted in the first part of Table 7 according to their total energies. Tabulated together are the numbers of heteroatomic (Ag−Al) contacts located in the first coordination environments among these models. It is evident that the more Ag−Al connections, especially shorter Ag−Al contacts, the lower the total energy is. This finding is noteworthy because, by contrast, when the molar ratio is around 1:1, Ag and Al atoms tend to segregate in the binary system into an hcp-type δ-phase (22.85−41.93 atomic percent Al) and an fcc-phase (ca. 75.0−100 atomic percent Al).[34]

According to the results of the randomly structured Models **1**−**4**, the coloring schemes with the lowest total energy

(30) Müllmann, R; Mosel, B. D.; Eckert, H.; Pöttgen, R. *J. Solid State Chem.* **1998**, *137*, 174.
(31) Hossain, Z.; Nagarajan, R.; Etilé, M.; Godart, C.; Kappler, J. P.; Gupta, L. C.; Vijayaraghavan, R. *J. Magn. Magn. Mater.* **1995**, *150*, 223.
(32) Gimarc, B. M. *J. Am. Chem. Soc.* **1983**, *105*, 1979.
(33) Miller, G. J. *Eur. J. Inorg. Chem.* **1998**, 523.
(34) *ASM Handbooks Online*; available from http://products.asminternational.org/hbk/index (accessed Aug 2008).

Table 5. Comparison in Unit Cell Size and vec between $BaCd_{11}$-type RE−Ag−Al Ternaries

composition	lattice param *a* (Å)	lattice param *c* (Å)	$V_{unit\ cell}$ (Å^3)	vec	ref
$LaAg_{6.05}Al_{4.95}$[a]	11.065(2)	7.123(2)	872.1(2)	2.17	10d
$CeAg_{5.72-6.38}Al_{5.28-4.62}$[b]	11.0466(3)	7.1101(5)	867.63(6)	2.11−2.24	10a,10c
$PrAg_{5.9(1)}Al_{5.1(1)}$	11.0262(2)	7.0979(2)	862.94(2)	2.20	10g
$EuAg_{4.96(4)}Al_{6.04(4)}$	11.0549(17)	7.1301(15)	871.4(3)	2.28	
$EuAg_{5.07(4)}Al_{5.93(4)}$	11.0613(10)	7.1302(9)	872.4(2)	2.27	
$EuAg_{5.80(7)}Al_{5.20(7)}$	11.0907(11)	7.1174(10)	875.5(2)	2.13	
$EuAg_{6.02(5)}Al_{4.98(5)}$	11.102(3)	7.125(2)	878.3(4)	2.09	

[a] The uncertainties of composition were not reported. [b] The lattice parameters correspond to the composition of $CeAg_{5.4(3)}Al_{4.6(3)}$.

Table 6. Mulliken Populations Calculated with Uniform Reference Frames at 24 Valence Electrons per f.u.

	$EuAg_{11}$		$EuAl_{11}$	
4a	Eu	0.573	Eu	0.073
4b	Ag1	2.104	Al1	2.083
8d	Ag2	2.112	Al2	2.252
32i	Ag3	2.138	Al3	2.168

Table 7. Total Energies and the Number of Ag−Al Contacts of Calculation Models

model	E_{total} (eV)	Ag−Al contacts per unit cell <2.70 Å	<2.80 Å	<3.00 Å
1	6.923	0	64	104
2	5.899	16	64	88
3	4.879	16	72	104
4	2.909	32	64	104
5	0	32	96	128

should be the ones with the maximal number of Ag−Al contacts. A straightforward way to find them is to generate all coloring schemes and count their Ag−Al contacts. This was realized with the help of a short program, the details of which are provided in the Supporting Information. By fixing the composition at $EuAg_6Al_5$, the maximal number of Ag−Al contacts was found within one specific coloring scheme, numbered as model **5**, in which one-half of the Eu atoms are coordinated as shown in Figure 4e and the other half as shown in Figure 4f. The number of Ag−Al connections in model **5** is listed in the last row of Table 7, together with the calculated total energy, which is, as expected, lower than the total energies of the randomly chosen models **1**−**4**. Therefore, model **5**, which has the maximal number of Ag−Al contacts, is indeed energetically favorable. Moreover, by comparing Figure 4 and Figure 2c, it can be seen that the original 4b site in Model **5** is assigned completely to Ag (the site occupancy Ag:Al = 1:0), and the original 8d and 32i sites are both half-filled by Ag atoms and Al atoms (Ag:Al = 0.5:0.5). This is very close to the experimentally observed site occupancies listed in Table 3. All of these results reveal that model **5** is a good simulation of the experimental structure and, thus, an appropriate computational model for further chemical bonding analysis.

Density of States and Bonding Characteristics. DOS and COHP curves were calculated for Model **5** and plotted in Figure 5. The overall shape of the DOS curve follows a parabola, which is the feature of the free-electron DOS, superimposed with the large peak of Ag 4d bands at ca. −8 to −3 eV as well as a state-deficient region, i.e., a pseudogap, at ca. −1 to +2 eV. The Fermi levels corresponding to vec values 2.1−2.3 e$^-$ per atom fall into this pseudogap.

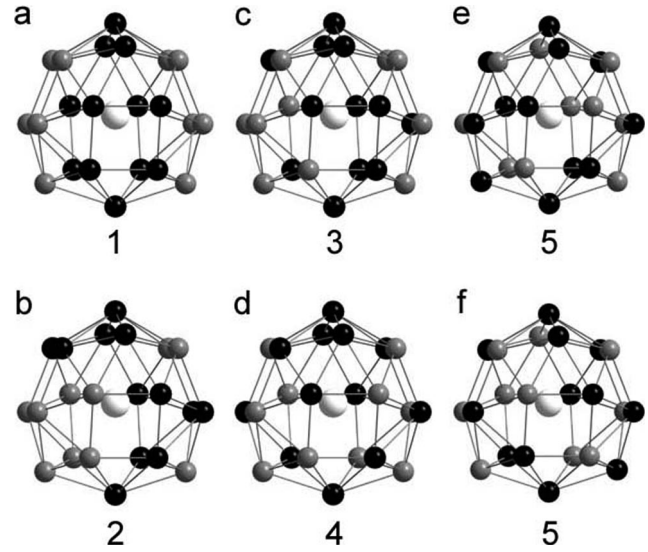

Figure 4. Coordination environments of the Eu atoms in the five calculation models. All models have the same composition, $EuAg_6Al_5$. Models **1**−**4** were randomly established. Model **5** was established by maximizing the number of Ag−Al contacts.

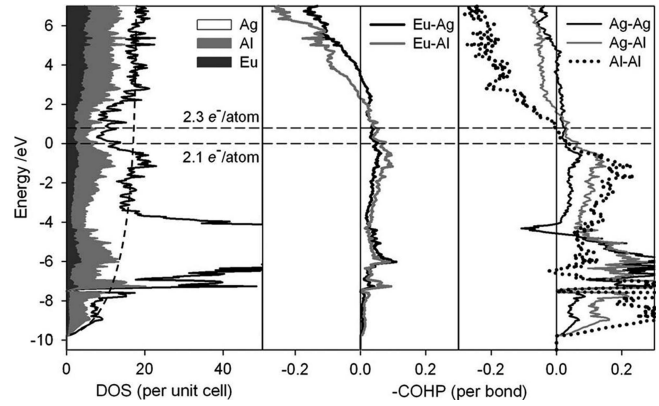

Figure 5. DOS and COHP curves calculated from model **5**. The dashed parabolic line shows the DOS curve of free electrons.

The COHP curves reveal that strong bonding interactions exist between Ag/Al−Ag/Al sites (integrated COHP values at vec = 2.1 e$^-$ per atom are: Ag−Ag, 0.83; Ag−Al, 1.27; Al−Al, 1.42), but that the Eu−Ag/Al orbital interactions are weakly bonding (integrated COHP values at vec = 2.1 e$^-$ per atom are: Eu−Ag, 0.30; Eu−Al, 0.38). As shown in the far right of Figure 5, the Fermi levels for the vec = 2.1−2.3 e$^-$ per atom are located very near the bonding−antibonding crossover for the Al−Al interactions, just below the bonding−antibonding crossover for the Ag−Al interactions and within the nearly nonbonding region for the Ag−Ag COHP curve. Specifically, the upper limit of allowed vec

values, ca. 2.3 e^- per atom, is set by the homoatomic Al−Al contacts. So, the orbital interactions within the Ag/Al network are essentially optimized for the $BaCd_{11}$-type phases. Any deviation in vec will destroy this bonding optimization and, thus, potentially destabilize the structure. This explains why the $BaCd_{11}$-type structure is specifically stabilized in RE−Ag−Al ternaries at the vec of ca. 2.1−2.3 e^- per atom.

Conclusions

$EuAg_xAl_{11-x}$ phases adopting the $BaCd_{11}$-type structure were experimentally and theoretically investigated. Ag and Al atoms share the same sites within the structure, although not entirely in a statistical manner. The 4b site prefers Ag to Al, which can be rationalized through a Mulliken population analysis with Extended Hückel calculations. First-principles calculations with TB-LMTO-ASA approach revealed that Ag and Al tend to be distributed to maximize the number of heteroatomic contacts. A computational model to analyze chemical bonding factors was established accordingly. The computational results successfully explained why this $BaCd_{11}$-type structure $EuAg_xA_{11-x}$ is stable only at vec = 2.1−2.3 e^- per atom. Further questions under investigation include the competition between $BaCd_{11}$-type and $BaHg_{11}$-type structures in Eu−Ag−Al ternary system.

Acknowledgment. This work is supported by NSF DMR 02-441092 and 06-05949. The authors thank Sumohan Misra and Prof. Vitalij K. Pecharsky for magnetization measurements.

Supporting Information Available: The powder XRD patterns of $EuAg_xAl_{11-x}$ (when $x = 3$, 4, 7, and 8), the single-crystal XRD results of "$EuAg_6Al_5$" samples, and the method of maximizing the number of Ag−Al contacts in $EuAg_6Al_5$ (PDF). This material is available free of charge via the Internet at http://pubs.acs.org.

CM803021U